Loughborough
University

This item was submitted to Loughborough's Institutional Repository (https://dspace.lboro.ac.uk/) by the author and is made available under the following Creative Commons Licence conditions.

For the full text of this licence, please go to:
http://creativecommons.org/licenses/by-nc-nd/2.5/

Modelling gas flow pressure gradients in gelcast ceramic foam diesel particulate filters

E M Adigio[1], **J G P Binner**[2], **C P Garner**[1]*, **R J Hague**[1], and **A M Williams**[1]

[1]Wolfson School of Mechanical and Manufacturing Engineering, Loughborough University, Loughborough, UK
[2]Institute of Polymer Technology and Materials Engineering, Loughborough University, Loughborough, UK

Abstract: New mathematical models are proposed that predict fluid flow pressure gradients in gelcast ceramic foam diesel exhaust particulate filters by considering the foam structure conceptually as serially connected orifices. The resulting multiple orifice mathematical (MOM) model is based on the sum of a viscous term derived from an extended Ergun model and the kinetic energy loss derived from the Bernoulli and conservation of mass equations. The MOM model was calibrated using experimental data obtained from measuring the air flowrate and pressure drop across a physical large-scale three-dimensional model of a cellular foam structure produced using rapid manufacturing techniques. The calibrated model was then validated using fluid flow data obtained from gelcast ceramic foam filters of various cell sizes and was found to require no empirical recalibration for each gelcast ceramic foam sample. The MOM model for clean filters was extended to predict pressure gradients of filters loaded with particulate matter (PM). The prediction of pressure gradients through gelcast ceramic filters using the MOM model for clean and PM-loaded cases was shown to be in reasonable agreement with experimental data. The models were finally applied to design a filter for a turbocharged, charge-cooled, 2.0l, four-stroke, common rail, direct injection passenger car diesel engine.

Keywords: fluid flow, diesel, engine, particulate, filter, pressure, exhaust, model, after-treatment, emissions, ceramic foam

1 INTRODUCTION

Diesel engine exhaust emissions have been reported to affect human health adversely, as well as contribute to acid rain and reduced atmospheric visibility [1, 2]. Consequently, governments including those in the United States, Japan, and many European countries are enforcing stringent standards to reduce diesel engine emissions, including particulate matter (PM). In order to meet these vehicle emission standards a number of engineering solutions have been investigated for reducing diesel engine PM emissions, often focusing around exhaust diesel particulate filter (DPF) technology [3, 4].

Mathematical modelling is increasingly becoming an engineering tool to understand, predict, and control DPF systems. These systems have aided the evaluation of filtration efficiency and the pressure drop across the filter. The latter affects engine performance measures such as power and fuel economy. Predicting these parameters allows faster design of DPF systems and reduces development cost. Recent developments in ceramic foam filtration technology have led to the manufacture of gelcast ceramic foams [5] that offer the ability to tailor pore geometry and overall filter geometry to maximize filtration efficiency and minimize exhaust gas flow back-pressure. These ceramic foams can be manufactured in a wide variety of shapes and sizes. These attributes make them attractive for automotive engine applications where there are acute size and shape limitations. This paper reports new work in modelling pressure gradients through gelcast cellular ceramic foam filters.

*Corresponding author: Wolfson School of Mechanical and Manufacturing Engineering, Loughborough University, Loughborough, Leicestershire, LE11 3TU, UK. email: c.p.garner@lboro.ac.uk

Honeycomb wall-flow filters [4–8] are, to date, the most commonly used type of DPF. Most of the validated models on pressure drop across DPFs are based on honeycomb wall-flow filters [9–15]. The modelling of porous media such as ceramic foam filters has been of interest to significantly fewer researchers. Many reported research findings on ceramic foam modelling are based on early work with respect to pressure drop relationships in spherical packed beds [16, 17]. For example, Innocentini *et al.* [18] and Richardson *et al.* [19] developed their models by adapting the model first developed by Ergun [17] to the foam filter structure by redefining a number of parameters based on foam geometry (e.g. cell diameter and specific filter surface area). Pontikakis *et al.* [20] reported the development of a mathematical model for the prediction of pressure drop across reticulated foam filters that differ significantly in their pore structure compared with the gelcast ceramic foams considered in the current paper, as illustrated in Fig. 1 [21, 22]. They assumed that the struts that form the solid framework of foam filters can be modelled as fibre elements, an assumption that cannot be applied to gelcast ceramic foams. Although the reported results were considered satisfactory, their models required the experimental determination of the permeability of the foam filter. Nevertheless, the well-defined Ergun model offers a sound fundamental relationship and is adapted in the present work to suit the gelcast ceramic foam filter structures for defining the viscous pressure losses. In addition here, a new approach to the kinetic losses is developed to allow calculation of overall pressure gradients. The resulting model, referred to as the multiple orifice mathematical (MOM) model, was calibrated and validated using fluid flow data in physical scale model foams and real gelcast ceramic foam samples respectively.

Significant progress has been made towards the understanding of transient behaviour of deep bed filtration in fibrous filters [23, 24] and granular filters [25]. However, few studies have been published on PM-loaded foam filters and, in particular, gelcast ceramic foam filters. The pressure drop across a PM-loaded filter as proposed and used by some researchers [9, 26–28] is the sum of the pressure drop across the clean filter plus the flow resistance of the trapped particles, with the assumption that the deposition of the particles in the filter is uniform. This approach is suitable for filters that exhibit cake filtration, since the Darcy law can be applied to the flow through the cake in a similar manner to the filter itself [9] but not in the case of deep-bed filtration. An alternative model suitable for loaded gelcast ceramic foams is therefore developed.

2 DEVELOPMENT OF THE MOM MODEL

In order to model fluid flow through ceramic foam filters in a computationally efficient manner, the fairly random foam structures are best represented conceptually by a well-defined model structure. For example, in the study of fluid flow in granular filters, some researchers [29] have represented the filter structure with constricted tubes, which are similar to the structure of the ceramic foam filter.

The cell arrangement adopted in the present research is based on the observation of a study of the microstructure of the gelcast ceramic foam filters exhibiting a structure closely comparable to a face-centred cubic lattice [30]. This is a good
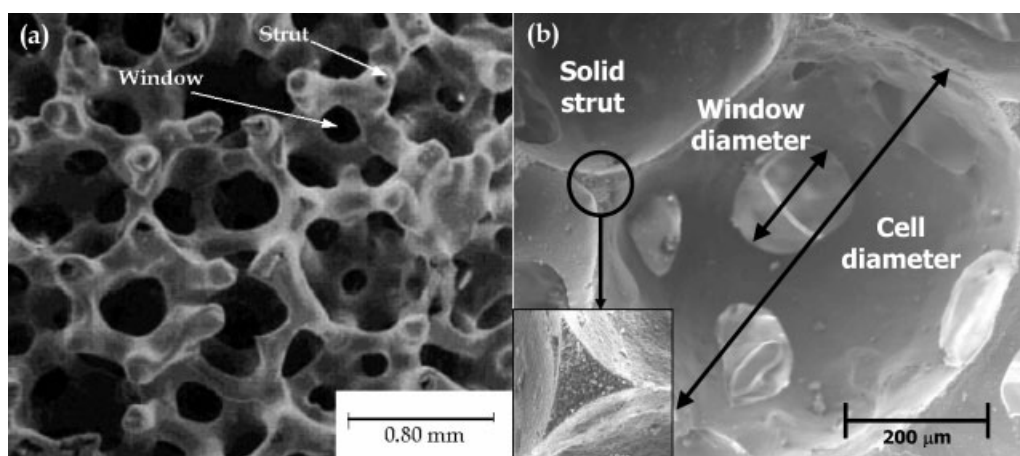

Fig. 1 Examples of (a) reticulated form structure [21] and (b) gelcast ceramic foam structure [22]

representation of the gelcast ceramic foam structure (i.e. spherical open pores connected by open windows) as shown in Fig. 1(b). Although there has been no previously reported application of the classical equations of fluid flow on a model structure formed by an assemblage of open spherical cells, its resemblance to the foam filters made it an attractive option.

The face-centred cubic lattice can be described by rows of cells arranged such that each cell is connected to 12 neighbouring cells. Assuming that the fluid flow across the filter is unidirectional, the structure can be simplified to a single row of interconnected cells as illustrated in Fig. 2. The fluid flow through the filter continuously experiences contraction and expansion owing to the alternating arrangement of windows and cells, like fluid flow through a series of constricted tubes or orifices.

For the potentially high-gas-flow velocities experienced in diesel engine exhaust flows, the total pressure drop is the sum of viscous energy loss associated with flow across a surface and the kinetic energy loss associated with the restrictions. That is, the total pressure drop (Δp), across the filter can be expressed as

$$\Delta p = \Delta p_{\text{vis}} + \Delta p_{\text{kin}} \tag{1}$$

where Δp_{vis} is the viscous pressure drop and Δp_{kin} is the kinetic pressure drop.

2.1 Viscous pressure losses

The viscous pressure drop was derived by applying the Ergun model [17] that defines the pressure gradient as a function of the superficial velocity u, and the specific surface area S_V of a packed bed, which is given by

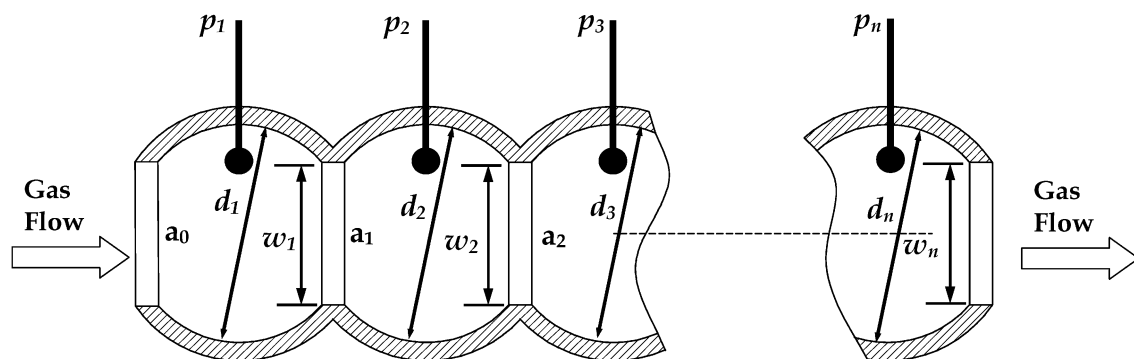$$\frac{\Delta p_{\text{vis}}}{L} = 2\alpha \frac{(1-\varepsilon)^2}{\varepsilon^3} \mu u S_V^2 \tag{2}$$

where α is a correction factor applied to account for the tortuous flow path of the fluid through the packed bed, $\Delta p_{\text{vis}}/L$ is the pressure gradient, ε is the filter porosity, and μ is the viscosity of the gas. By defining the specific surface area with respect to the parameters of the ceramic foam using the face-centred cubic lattice conceptual model, this relationship can be defined specifically for the gelcast ceramic foam filters.

The specific surface area S_V is the wetted surface (i.e. the surface exposed to the fluid flowing through the filter) per unit volume of filter material. Considering a unit volume of filter, the total wetted surface per unit volume is the product of the number of cells N and the wetted surface area of a cell S, i.e.

$$\text{Total wetted surface area} = NS = \frac{\varepsilon S}{V_{\text{CELL}}} \tag{3}$$

where V_{CELL} is the open volume of a single pore. The volume of filter material per unit filter volume V_{mat} is expressed as

$$V_{\text{mat}} = 1 - \varepsilon \tag{4}$$

Solving for the specific surface area S_V from equations (3) and (4) gives

$$S_V = \frac{S\varepsilon}{V_{\text{CELL}}(1-\varepsilon)} \tag{5}$$

In this analysis the preferential flow direction leads to the dominant flow through two of the 12 windows. Therefore, the shared surface areas of ten of the adjacent cells are added to the total wetted surface area of the cell. The surface area of a sphere of diameter d is given as πd^2. The surface area truncated by one neighbouring cell S_{TR} is given as πdh, where, as illustrated geometrically in Fig. 3, h can be expressed as

Fig. 2 Conceptual MOM model of the ceramic foam filter

$$h = \frac{d}{2} - \frac{\sqrt{d^2 - w^2}}{2} = \frac{d}{2}\left(1 - \sqrt{1 - w/d}\right) \tag{6}$$

where w is the connecting window diameter. Therefore, the surface area truncated by a single neighbouring cell can be rewritten as

$$S_{TR} = \pi \frac{d^2}{2}\left(1 - \sqrt{1 - k^2}\right) \tag{7}$$

where $k = w/d$.

Hence, the total truncated surface area from the 12 neighbouring cells can be written as

$$\text{Total truncated area} = 12 S_{TR} = 6\pi d^2\left(1 - \sqrt{1 - k^2}\right) \tag{8}$$

Furthermore, the ten shared surface areas bounding the windows of diameter w can be written as $5\pi w^2/2$. Finally, the wetted surface area S is, therefore, given by

$$S = \pi d^2 \left[1 - 6\left(1 - \sqrt{1 - k^2}\right) + 5k^2/2\right] \tag{9}$$

The volume of the cell V_{CELL} is equivalent to the volume of a spherical cell V_S minus the volumes truncated by the 12 neighbouring cells V_C, i.e.

$$V_{CELL} = V_S - V_C \tag{10}$$

The volume of the spherical cell is given as

$$V_S = \pi \frac{d^3}{6} \tag{11}$$

The truncated volume can be expressed as

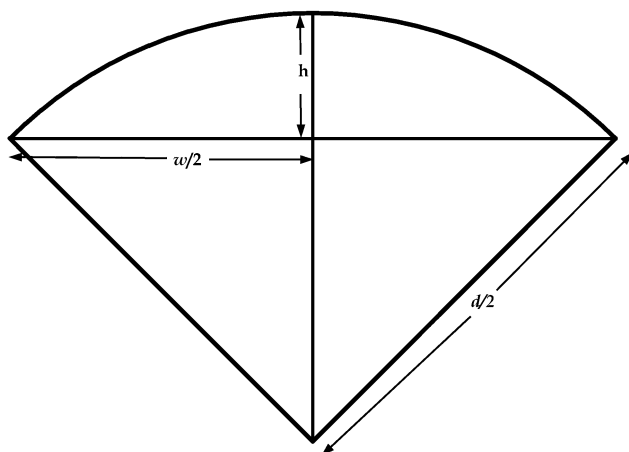**Fig. 3**   Diagram of a sector of a cell

$$V_C = 12\left[\frac{\pi}{6}\left(3\frac{w^2}{4} + h^2\right)h\right] \tag{12}$$

Substituting the value of h from equation (6) and simplifying yields

$$V_C = \frac{\pi d^3}{4}\left(3k^2 + B^2\right)B \tag{13}$$

where $B = 1 - \sqrt{1 - k^2}$. Hence, substituting V_S and V_C in equation (10) gives the expression for the volume of the cell as

$$V_{CELL} = \frac{\pi d^3}{12}\left[2 - 3\left(3k^2 + B^2\right)B\right] \tag{14}$$

By substituting the values of S and V_{CELL} in equation (5) the specific surface area can be written as

$$S_V = \frac{12\left(1 - 6B + 5k^2/2\right)\varepsilon}{d\left[2 - 3B\left(3k^2 + B^2\right)\right](1 - \varepsilon)} \tag{15}$$

Finally, substituting S_V in equation (2) yields a working equation for calculation of viscous pressure losses in gelcast ceramic foam filters as

$$\frac{\Delta p_{vis}}{L} = \left\{\frac{12\left(1 - 6B + 5k^2/2\right)}{\left[2 - 3B\left(3k^2 + B^2\right)\right]}\right\}^2 \frac{\alpha \mu u}{d^2 \varepsilon} \tag{16}$$

where α is the viscous pressure loss correction coefficient, which is chosen as $\alpha = 5$ as suggested by Macdonald *et al.* [**31**]. All other terms are either known or can be directly measured from the foam sample.

2.2 Kinetic pressure losses

Treating the window as an orifice-type restriction to the flow, the Bernoulli equation and mass conservation law can be used to derive the well-known relationship between the fluid flowrate and the pressure drop across each window

$$q_{ideal} = A_W \sqrt{\frac{2\Delta p}{\rho\left[1 - \left(A_W^2/A_0^2\right)\right]}} \tag{17}$$

where q_{ideal} is the ideal fluid flowrate, Δp is the pressure drop across the window, A_0 is the equivalent tube cross-sectional area, and A_W is the window cross-sectional area. To account for non-ideal flow (e.g. turbulent losses) a window orifice flow coefficient, β, is included in equation (17) to give the

actual fluid flowrate, q, as

$$q = \beta A_\text{w} \sqrt{\frac{2\Delta p}{\rho\left[1 - (A_\text{w}^2/A_\text{o}^2)\right]}} \tag{18}$$

Rearranging for the pressure drop gives

$$\Delta p = \frac{\rho q^2}{2\beta^2 A_\text{w}^2}\left[1 - \frac{A_\text{w}^2}{A_\text{o}^2}\right] \tag{19}$$

The total kinetic pressure drop Δp_kin across the filter is the sum of the pressure drops across all the individual windows; that is, the pressure drop owing to the kinetic energy loss can be expressed as

$$\Delta p_\text{kin} = \Delta p_{12} + \Delta p_{23} + \Delta p_{34} + \ldots + \Delta p_{m,m+1}$$

$$= \sum_{M=1}^{M} \Delta p_{m,m+1} = M\frac{\rho q^2}{2\beta^2 A_\text{w}^2}\left(1 - \frac{A_\text{w}^2}{A_\text{o}^2}\right) \tag{20}$$

or

$$\Delta p_\text{kin} = M\frac{\rho q^2}{2\beta^2 A_\text{w}^2}\left(1 - \frac{w^4}{d_\text{o}^4}\right) \tag{21}$$

where d_o is the diameter of an equivalent tube of the row of cells and M is the number of orifices in the row of cells across the filter, given by

$$M = \frac{L}{\sqrt{d^2 - w^2}} \tag{22}$$

and w is the window diameter, d is the cell diameter, and L is the filter length.

The fluid flowrate through a single row of cells q is a fraction of the total fluid flowrate Q through the filter, which is calculated as follows. Knowing that there are N_row rows of cells in the cross-section of the filter and the volume of fluid flowing through the filter per unit time is Q, the fluid flow in a single row of cells per unit time q is expressed as

$$q = \frac{Q}{N_\text{row}} \tag{23}$$

The porosity of the filter for cylindrical cells can be expressed as

$$\varepsilon = \frac{A_\text{flow}L}{A_\text{filt}L}$$

$$= \frac{N_\text{row}\pi d_\text{o}^2}{4A_\text{filt}}$$

or

$$\varepsilon A_\text{filt} = N_\text{row}\pi\frac{d_\text{o}^2}{4} \tag{24}$$

where A_filt is the cross-sectional area of the filter.

Solving for N_row in equation (26) and substituting A_filt for $\pi D^2/4$ yields

$$N_\text{row} = \frac{\varepsilon D^2}{d_\text{o}^2} \tag{25}$$

where D is the filter diameter. Therefore, substituting N_row in equation (23) gives the expression

$$q = \frac{d_\text{o}^2}{\varepsilon D^2}Q \tag{26}$$

The relationship between the cell diameter d and the equivalent tube diameter d_o is such that the volume of the tube is equal to the sum of the volume of the row of cells, i.e.

$$\pi\frac{d_\text{o}^2}{4}L = MV_\text{CELL} \tag{27}$$

Hence, substituting V_CELL from equation (14) and M from equation (22), and solving for d_o gives the expression

$$d_\text{o} = \left[\frac{d^3\left(2 - 3B\left(3k^2 + B^2\right)\right)}{3\sqrt{d^2 - w^2}}\right]^{0.5} \tag{28}$$

The kinetic pressure gradient across gelcast ceramic foam filters can now be written as

$$\frac{\Delta p_\text{kin}}{L} = \frac{\left(1 - w^4/d_\text{o}^4\right)}{L\sqrt{d^2 - w^2}}\left(\frac{d_\text{o}^2}{\beta\pi\varepsilon D^2 w^2}\right)^2 8\rho Q^2 \tag{29}$$

2.3 Working equations

Knowing that the velocity of fluid flowing through the row of cells, u, can be expressed as

$$u = \frac{4q}{\pi d_\text{o}^2} = \frac{4}{\pi d_\text{o}^2}\frac{\pi d_\text{o}^2}{4\varepsilon}\frac{4Q}{D^2\pi} \tag{30}$$

or

$$u = \frac{4Q}{\varepsilon\pi D^2} \tag{31}$$

the total pressure gradient can be expressed by substituting for the viscous losses, equation (16), and

kinetic losses, equation (29), i.e.

$$\frac{\Delta p}{L} = \frac{\alpha\mu 4(1-\varepsilon)^2}{D^2\pi\varepsilon^3} S_{\mathrm{v}}^2 Q$$
$$+ \frac{(1-w^4/d_{\mathrm{o}}^4)}{L\sqrt{d^2-w^2}} \left(\frac{d_{\mathrm{o}}^2}{\beta\pi\varepsilon D^2 w^2}\right)^2 8\rho Q^2$$

where

$$d_{\mathrm{o}} = \left\{\frac{d^3\left[2-3B(3k^2+B^2)\right]}{3\sqrt{d^2-w^2}}\right\}^{0.5}$$

$$B = 1 - \sqrt{1-k^2} \quad \text{and} \quad k = w/d \qquad (32)$$

and S_{V} is the specific surface area of the foam filter defined earlier in equation (15).

The viscous pressure loss correction coefficient is $\alpha = 5$ as suggested by Macdonald *et al.* [**31**]. This leaves the kinetic correction coefficient β that needs to be defined experimentally. Importantly, these coefficients are independent of the filter microstructure and macrostructure (cell diameter, window size, and the fluid flowrate).

3 CLEAN FILTER MODEL CALIBRATION AND VALIDATION

3.1 Experimental set-up

The model required validation using a number of ceramic foam filter samples, the details of which are shown in Table 1. Owing to the manufacturing process there is a spread of pore and window diameters throughout the foams [**32**]. The data presented are the statistical means of ~ 500 optical measurements of pore and window diameter. An

Table 1 Cellular foam filter samples and their parameters

Type of filter	Mean cell size, d (mm)	Mean window size, w (mm)	Porosity, ε (%)
243AL-E	0.75	0.233	88
243AL-F	0.50	0.152	87
243AL-G	0.20	0.085	86
A44C7	0.85	0.221	80
A44C11	0.25	0.065	80
A44C6	0.25	0.075	86
A44C4	0.35	0.105	86
A44C1	0.75	0.277	88
A44C10	0.40	0.092	80
A44	0.261	0.068	80
A44C2	0.65	0.221	88
A103M	0.27	0.070	81.8
A103Z6	0.29	0.081	82.6
A85M	0.27	0.07	80.5
A103ZI	0.41	0.111	83.1

experimental rig was constructed to measure the pressure drop across the filter samples, the flowrates through the samples, and the temperature and absolute pressure of the fluid at the inlet (as shown in Fig. 4). Flowrates were measured using a calibrated orifice flow meter designed and assembled in accordance to the ISO 5167 standard [**33**]. A flow conditioner straightened the swirling air flow and reduced the pulsating effect from the centrifugal blower. The absolute pressure and temperature were measured before the filter holder to determine the density of the air. The experiments were repeated three times on each sample to evaluate experimental error.

In order to determine the constants in equation (32) a series of experiments was carried out using physical scale model foams. A 10:1 idealized physical scale model based on the face-centred cubic lattice was produced using the stereolithography process. Its structure is illustrated by the computer-aided design drawing in Fig. 5. Pressure tappings were incorporated as part of the manufactured three-
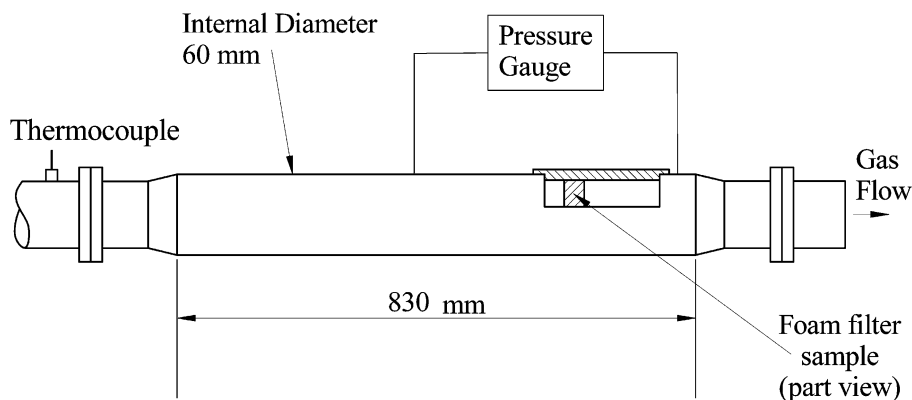

Fig. 4 Schematic diagram of a flow rig foam filter sample holder

dimensional structure to allow accurate pressure measurements to be taken from individual cells. The advantage of using the stereolithography to produce the scale model lies in the accuracy of the process and the ability to produce complex geometries without the need to resort to mould tooling – therefore, the relatively complex structure of the filter could be manufactured comparatively easily. This would have been difficult to achieve with other manufacturing approaches, or indeed on a real ceramic foam sample.

3.2 Model calibration

The calibration of the MOM model required the determination of constant β so that the kinetic losses matched the experimental data obtained from the physical scale model foam. The MOM model was calibrated using the experimental data from a 25 mm-thick physical scale foam model. The value for kinetic correction coefficient β that gave the best fit became the constant correction coefficient of the mathematical model that was then validated with a range of real gelcast foam samples.

Figure 6 shows the resulting graph of pressure gradient as a function of fluid flowrate following calibration using the physical scale model. The value of the kinetic correction factor β corresponding to the fit was equal to 2.2. Therefore, the mathematical model can be rewritten after substituting the value β as

$$\frac{\Delta p}{L} = \frac{5\mu 4(1-\varepsilon)^2}{D^2 \pi \varepsilon^3} S_\mathrm{v}^2 Q$$
$$+ \frac{(1-w^4/d_\mathrm{o}^4)}{L\sqrt{d^2-w^2}} \left(\frac{d_\mathrm{o}^2}{2.2\pi\varepsilon D^2 w^2} \right)^2 8\rho Q^2 \qquad (33)$$
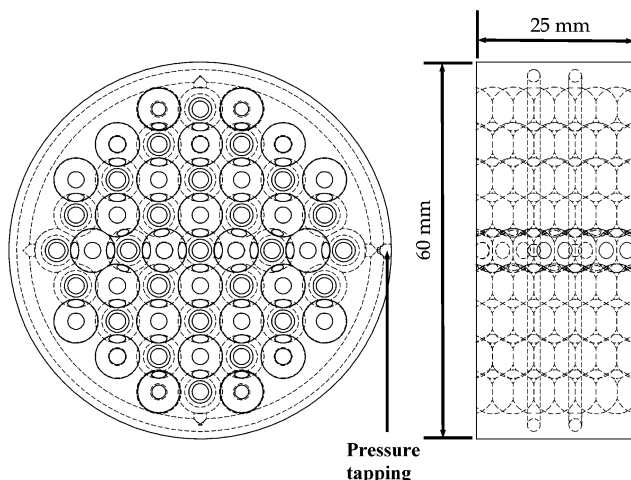

Fig. 5 Drawing of a physical scale model of a cellular foam filter manufactured using stereolithography
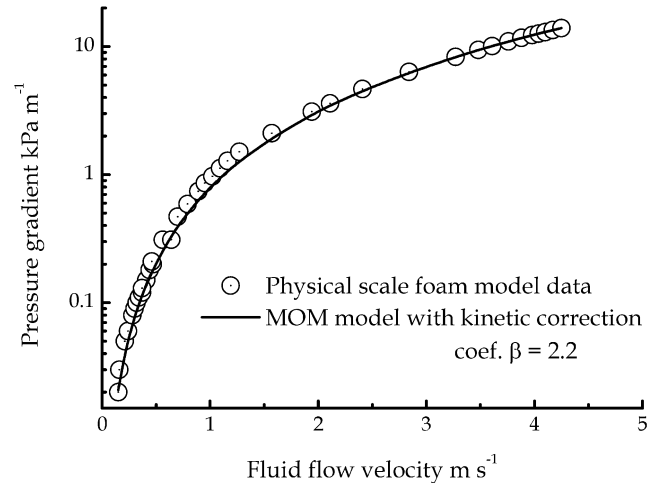

Fig. 6 Graph of pressure gradient versus fluid flowrate in a physical scale model foam sample for the calibration of the MOM model

The model calibration was repeated using data from the physical scale model foam of lengths 100 mm at different ranges of Reynolds number (*Re*), from 1 to 70. Values of correction coefficients obtained were found to be independent of the Reynolds number for this range and this implies that the MOM model is applicable to the wide range of pore sizes found in gelcast ceramic foams.

3.3 Validation of MOM model

The calibrated MOM model was validated by comparing the predicted pressure gradient with experimental results from the real gelcast ceramic foam samples. Figures 7 and 8 are graphs of pressure gradients versus mass flowrate. The results show that the proposed MOM model is a promising tool for the prediction of pressure gradients of clean gelcast ceramic foam filters where the porosity and the cell diameter are known. Importantly, the MOM model does not require individual calibration for each foam sample.

4 MODELLING PM-LOADED GELCAST CERAMIC FOAM FILTERS

The MOM model was further developed to model the effect of PM loading in the foam. Scanning electron microscope (SEM) imaging of the window of a PM-loaded ceramic foam filter (see Fig. 9) revealed that the deposition of the PM is predominantly around the exit window edge of each cell. From these observations the PM-loaded model was developed.
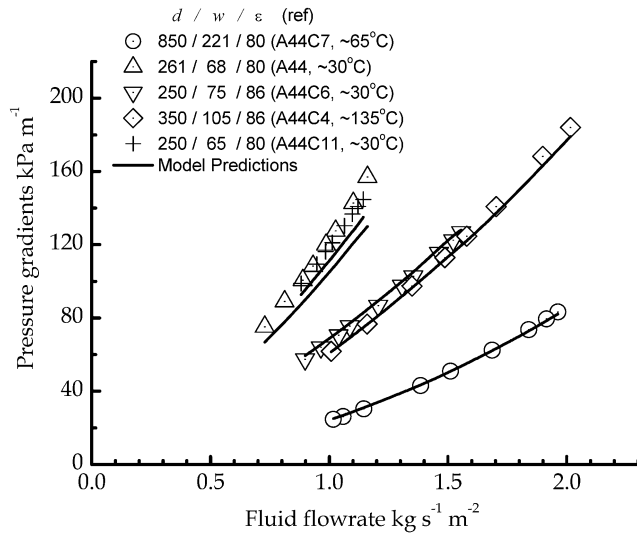
Fig. 7 Graphs of pressure gradients versus fluid flowrate in samples of gelcast ceramic foams, comparing experimental data with the MOM model, A44C series of filter samples, and the alumina foam filter sample
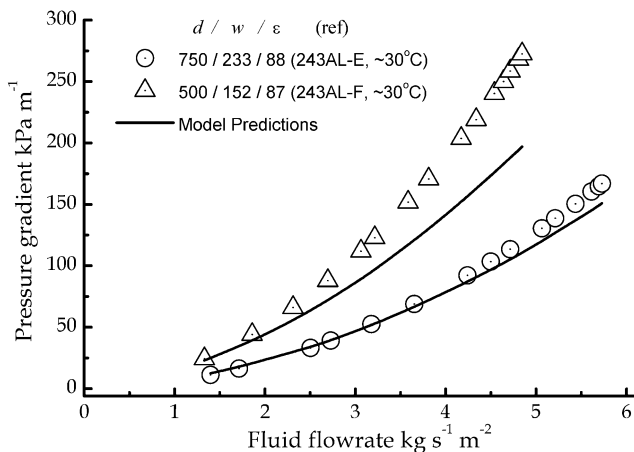

Fig. 8 Graph of pressure gradient versus fluid flowrate in samples of gelcast ceramic foams, comparing experimental data with the MOM model, 243AL series of filter samples

Figure 10 shows a conceptual model of the PM loading within the cells adapted from the original MOM model. The shaded surface area when rotated around the x axis is the volume of PM deposit in the cell. The main effect of the PM layer is the reduction in the window size leading to increased kinetic losses.

The first stage was to calculate the PM volume, as this was needed to determine the filter PM loading. L_1 is a line coinciding with the upstream surface of the PM deposit initially considered to be perpen-

dicular to the radius of the cell passing through the circumference of the window. L'_1 is a rotation of L_1 through an angle ψ around A which is tuned when calibrating the PM-loaded MOM model with experimental data to establish the deposit surface inclination.

The point of intersection between the circle C and the line L'_1 and the intersection between lines L'_1 and L_2 are (x_1, y_1) and (x_2, y_2) respectively, r_1 is defined as the perpendicular distance from the line L_1 to the centre of the cell and h as the radius of the opening. The volume of the PM in the cell is, therefore, equal to the difference in volume generated by the arc of the circle between x_1 and x_2 around the x axis and the volume of the line L'_1 within the same boundary around the x axis.

The equation of the circle is

$$y = \sqrt{r^2 - x^2} \tag{34}$$

where r is the cell radius, i.e. $d/2$. The volume V_{arc} generated by the arc revolving around the x axis is determined from solving the following integration

$$V_{arc} = \pi \int_{x_1}^{x_2} (r^2 - x^2) \, \mathrm{d}x \tag{35}$$

yielding

$$V_{arc} = \pi \left[r^2 (x_2 - x_1) - \frac{x_2^3 - x_1^3}{3} \right] \tag{36}$$

The equation representing L_1 can then be written as

$$y = g_1 x + k_n \tag{37}$$

where g_1 and k_n are the gradient and the y axis point of intersection respectively. The volume V_{line} generated by the line revolving around the x axis is

$$V_{line} = \pi \int_{x_1}^{x_2} (g_1 x + k_n)^2 \, \mathrm{d}x \tag{38}$$

yielding

$$V_{line}$$
$$= \pi \left[g_1^2 \left(\frac{x_2^3 - x_1^3}{3} \right) + g_1 k_n (x_2^2 - x_1^2) + k_n^2 (x_2 - x_1) \right] \tag{39}$$

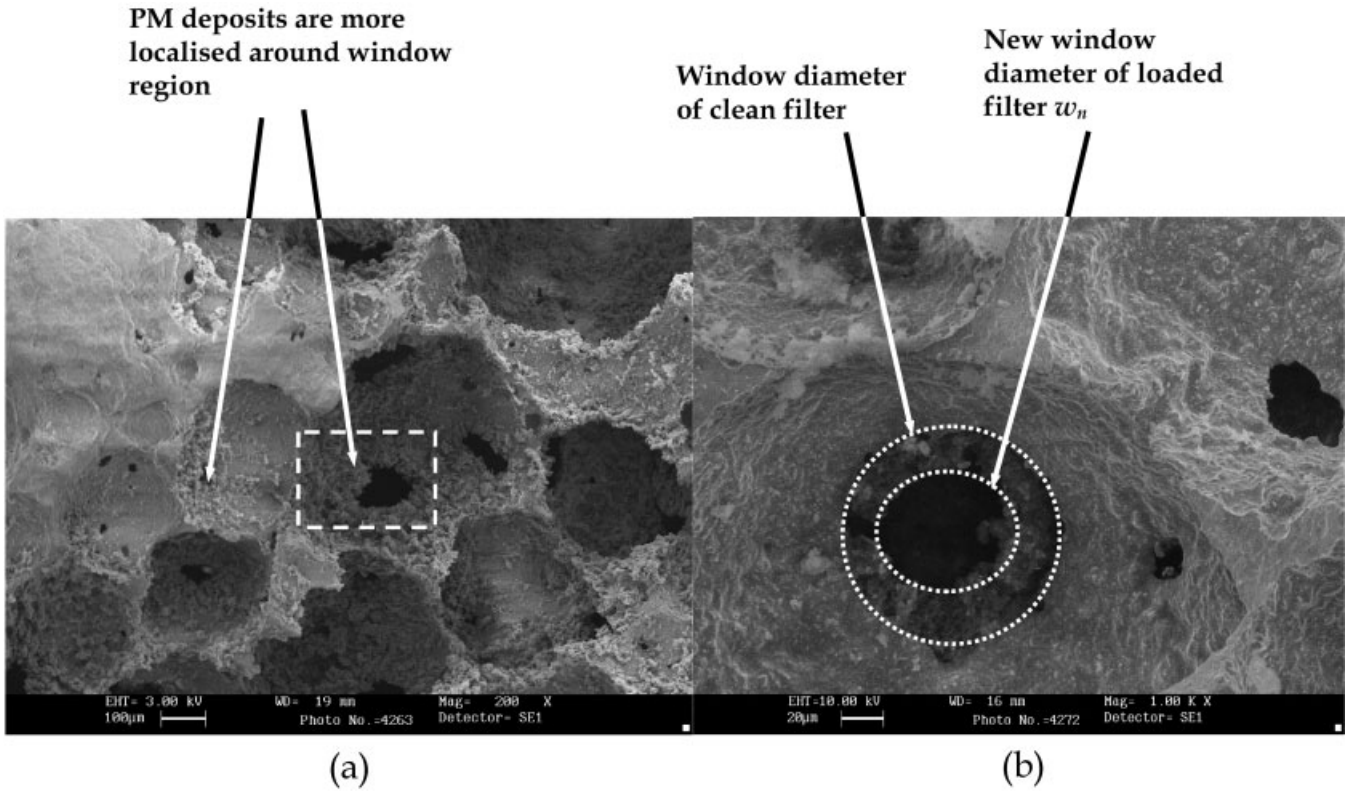Hence, the equivalent PM volume (V_{PM}) can be written as

Fig. 9 SEM image of loaded ceramic foam window: (a) showing deposits with magnification of 200; (b) showing deposition around window with magnification of 1000
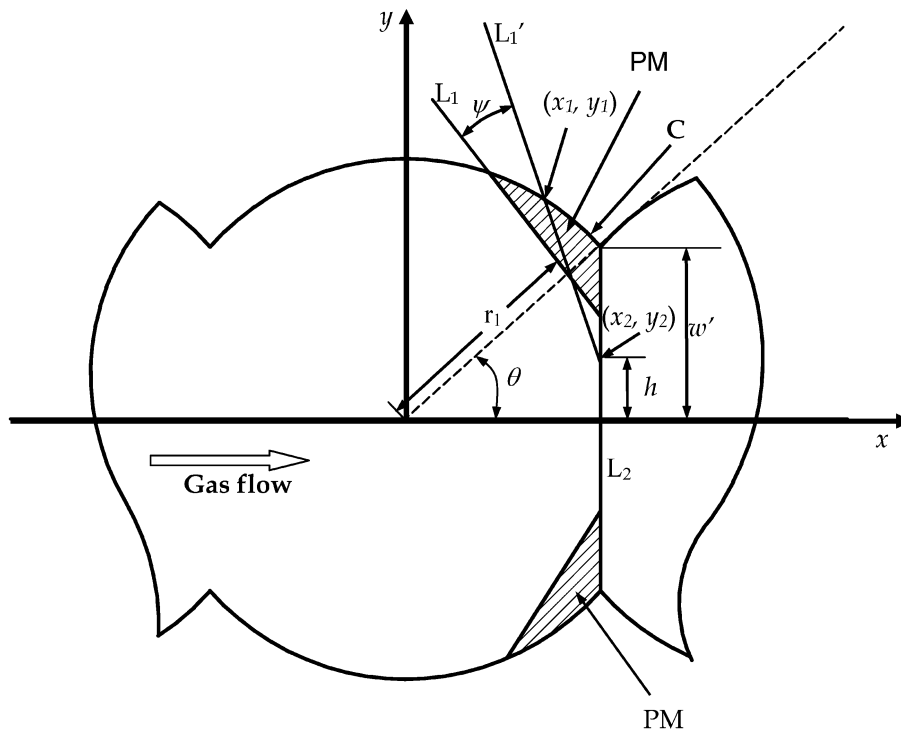

Fig. 10 Schematic diagram of deposition of PM in a foam cell, where deposition is lodged around the window and h is the radius of the opening of the loaded filter

$$V_{PM} = \pi \left[r^2 (x_2 - x_1) - \frac{x_2^3 - x_1^3}{3} - g_1^2 \left(\frac{x_2^3 - x_1^3}{3} \right) \right.$$
$$\left. - g_1 k_n \left(\frac{x_2^2 - x_1^2}{2} \right) - k_n^2 (x_2 - x_2) \right] \tag{40}$$

4.1 Determination of g_1, k_n, x_1, and x_2

The gradient of the line L_1 is given by

$$\tan\theta = \frac{w'}{\sqrt{r^2 - w'^2}} \tag{41}$$

and w' is the radius of the clean opening, i.e. $w/2$. As the line L_1 is arbitrarily chosen, the variation is considered to be in the calculation of g_1, the gradient of the line parallel to the surface of the deposit. The gradient of line L'_1, i.e. g_1 is determined as follows

$$g_1 = \tan\left(\theta + \frac{\pi}{2} - \psi\right)$$
$$= \frac{\cos\psi\cos\theta + \sin\psi\sin\theta}{\sin\psi\cos\theta - \cos\psi\sin\theta}$$

$$g_1 = \frac{(1/\tan\theta) + \tan\psi}{(\tan\psi/\tan\theta) - 1} = \frac{\sqrt{d^2 - w^2}/w + \tan\psi}{\sqrt{d^2 - w^2}/w\tan\psi - 1} \tag{42}$$

In order to determine k_n, the following relationship can be derived from Fig. 11

$$\frac{k_n}{\sin\left(\frac{\pi}{2} + \psi\right)} = \frac{r_1}{\sin(\theta - \psi)}$$

or

$$k_n = \frac{r_1}{\sin\theta - \tan\psi\cos\theta}$$

and

$$k_n = \frac{r_1}{(w/d) - \left(\sqrt{d^2 - w^2}/d\right)\tan\psi} \tag{43}$$

The value of x_1 is determined by equating equations (34) and (37) and solving the resulting equation for x, i.e.

$$\sqrt{r^2 - x^2} = g_1 x + k_n \tag{44}$$

which yields

$$x = \frac{-g_1 k_n \pm \sqrt{g_1^2 r^2 - k_n^2 + r^2}}{g_1^2 + 1} \tag{45}$$

From Fig. 11, the intersections of the line L_1 and the circle are the values of equation (43), i.e. x_1 and x'_1. The solution required in the analysis is x_1, which is the smaller of the two solutions of the quadratic equation, thus

$$x = \frac{-g_1 k_n - \sqrt{g_1^2 r^2 - k_n^2 + r^2}}{g_1^2 + 1} \tag{46}$$

Finally, the value of x_2, which is the intersection between L_1 and L_2, is determined from the intersection of L_2 with the x axis, i.e.

$$x_2 = \sqrt{r^2 - w'^2} = \frac{\sqrt{d^2 - w^2}}{2} \tag{47}$$

The value of the opening h in a loaded filter is determined by substituting the value of x_2 in the equation representing L'_1, equation (37), i.e.

$$h = g_1\sqrt{r^2 - w'^2} + k_n = g_1 \frac{\sqrt{d^2 - w^2}}{2} + k_n \tag{48}$$

Furthermore, as the PM occupies part of the void in the foam filter, the porosity is the ratio of the difference in volume of the initial void and the volume occupied by PM to the volume of the filter. The trapped PM occupies part of the void in the foam, thus, for unit volume of filter the porosity ε_n of the loaded filter is derived as follows

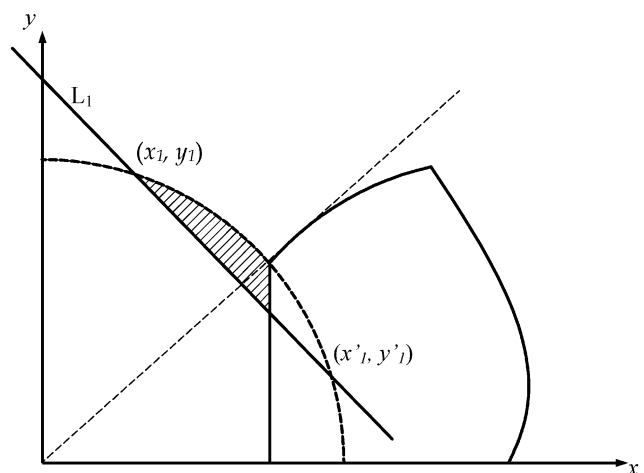$$\varepsilon_n = 1 - V_{mat} - V_p \tag{49}$$

Fig. 11 Diagram of intersection of L_1 and the cell circumference

where V_{mat} and V_p are the volume of the filter material and volume occupied by the particulates respectively. The volume occupied by particulates in terms of the specific loading σ of PM in the filter is written as

$$V_p = \frac{\sigma}{1 - \varepsilon_p} \tag{50}$$

Hence, replacing V_{mat} ($= 1 - \varepsilon$) and V_p in equation (49) yields

$$\varepsilon_n = 1 - (1 - \varepsilon) - \frac{\sigma}{1 - \varepsilon_p} \tag{51}$$

and

$$\varepsilon_n = \varepsilon - \frac{\sigma}{1 - \varepsilon_p} \tag{52}$$

where ε_p and ε are the deposited PM porosity and initial filter porosity respectively and σ is the ratio of the solid PM deposit (density $\sim 2200 \, kg \, m^{-3}$) to the filter volume. The porosity of the PM deposits, ε_p depends on the morphology of the deposits formed and changes in the course of deposition. However, as there are no reliable detailed data from foam filters, the same assumption made by Pontikakis *et al.* [20] was considered in this analysis, i.e. that $\varepsilon_p = 90$ per cent.

Having derived the correlation between the initial parameters and the PM-loaded parameters of the ceramic foam filter, the next subsection describes the determination of the volume of the PM deposited per unit foam cell.

4.2 Calculation of volume of PM per cell

Considering a unit volume of foam filter, the number of cells N is again written as follows

$$N = \frac{\varepsilon}{V_{CELL}} \tag{53}$$

where V_{CELL} is the cell volume. The volume of PM per unit cell V_{PM} is the volume of PM per unit filter volume divided by the number of cells in the unit filter volume, i.e.

$$V_{PM} = \frac{\sigma}{N} \tag{54}$$

Substituting N in equation (53), the expression for the PM volume per cell is

$$V_{PM} = \frac{\sigma V_{CELL}}{\varepsilon} \tag{55}$$

Finally, by equating equations (40) and (55) the value of the window size corresponding to a given load can be calculated after determining the perpendicular distance from the surface of the deposit to the centre of the cell r_1. The determination of r_1 is by iteration.

The range of possible values of r_1 is defined by

$$\left[\frac{d}{2} - \frac{w^2}{\sqrt{d^2 - w^2}} \right] \leqslant r_1 \leqslant \frac{d}{2} \tag{56}$$

The calculated value of the window diameter of the loaded foam filter w_n and the new porosity are then applied to the clean filter MOM model (i.e. equation (32)) to predict the pressure gradient for a given filter loading.

5 VALIDATING THE PM-LOADED MOM MODEL

5.1 Filter sample loading

Figure 12 shows a schematic diagram of an assembly of filter holder, foam filter samples, and the canister. A ceramic wall flow filter (WFF) of diameter 150 mm and length 75 mm was mounted downstream of the foam sample to butt the sample holder against the engine pressure. This prevented the sample from moving during the loading. The filter samples were loaded onto a 1100 series Perkins 4.4l, four cylinder four-stroke, turbocharged, after-cooled diesel engine at 1500 r/min, 82 Nm for 1.5 h. This corresponds to a temperature of $\sim 200\,^{\circ}C$ at a flowrate of 0.063 kg/s. Owing to the small filter diameter, a bypass valve was used to limit the sample flowrate to ~ 3 per cent of the total engine flow, maintaining reasonable flowrates through the filter of ~ 1 kg/s per m^2.
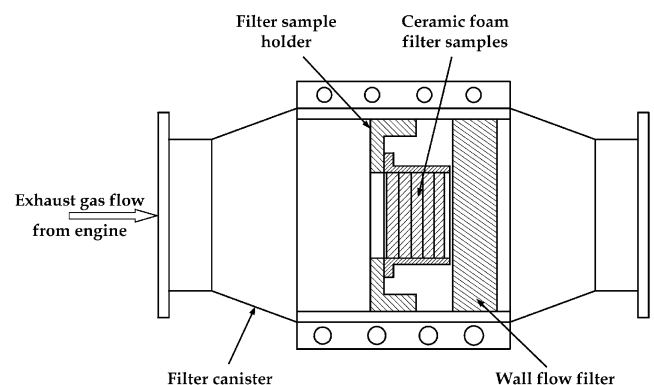

Fig. 12 Schematic diagram of filter sample holder for PM loading

Each sample of foam of length approximately 25 mm was carefully weighed on a Sartorius weighing machine to within ± 1 mg before mounting on the filter holder for the PM loading. The PM load was the difference between the clean and loaded filter samples. A compressed air supply was used to remove any loose PM and remnant gasket material prior to weighing the samples, to improve the accuracy of the PM loading measurement. This also removed any loose material that would have affected the flow and back-pressure data. The weighing of the clean and loaded foam filters for each loading experiment was carried out in the same ambient conditions to minimize environmental effects on mass measurements. Weighing of samples before and after the flow rig testing showed no change in mass as a result of the flow and back-pressure measurements.

The procedures for the fluid flow experiments used for the clean filters are applied to PM-loaded foam filters. Table 2 is a summary of the results showing the specific volume of PM (i.e. volume of PM per unit volume of filter).

5.2 Validation of improved PM-loaded foam filter MOM model

Using the PM loads reported in Table 2, the new filter parameters corresponding to each sample were calculated to include the porosity and the window diameter. The calculated values were then applied to the clean filter MOM model, while tuning the angle ψ. Curves from the resulting expression were compared with curves from the experimental data. Figures 13, 14, and 15 show graphs of pressure gradient versus fluid flowrate comparing the new PM-loaded MOM model with the experimental data with the angle of inclination of the PM loading $\psi = 5$ degrees. For comparative purposes, the model prediction of the clean gelcast ceramic foam filters of the same geometry and pore structure are shown in the figures.

6 APPLICATION OF MATHEMATICAL MODEL

There are a number of ways in which these models can be used, which include the evaluation of the

Table 2 The specific volume of PM of the foam filter samples

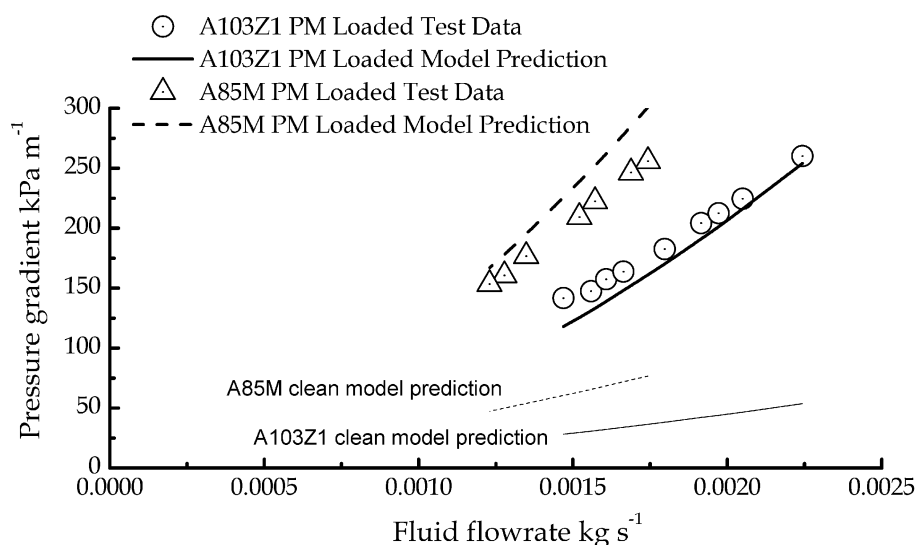| Filter type	Filter volume (m^3)	Clean filter mass (g)	Loaded filter mass (g)	PM load (g)	Specific volumetric PM load ($\times 10^{-3}$ l/l)
A44C6	5.82×10^{-5}	34.0497	34.099	0.0494	0.548
A44C4	6.12×10^{-5}	35.4965	35.531	0.0345	0.364
A44C2	6.2×10^{-5}	30.387	30.419	0.0325	0.331
A103Z6	4.9×10^{-5}	51.8861	51.924	0.0384	0.745
A85M	5.39×10^{-5}	40.4958	40.545	0.0493	0.631
A103ZI	5.1×10^{-5}	39.9735	40.041	0.0676	0.886

Fig. 13 Graph of pressure gradient versus fluid flowrate for PM-loaded ceramic foam filters, comparing model with experimental data
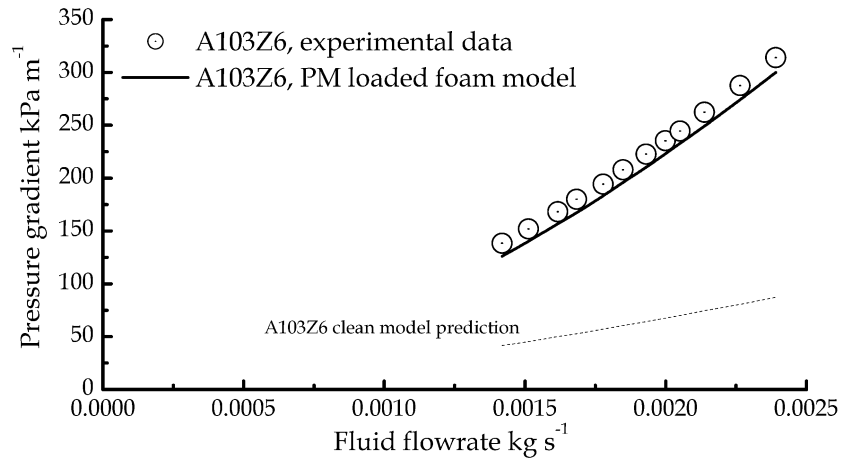
Fig. 14 Graph of pressure gradient versus fluid flowrate for PM-loaded ceramic foam filters, comparing model with experimental data
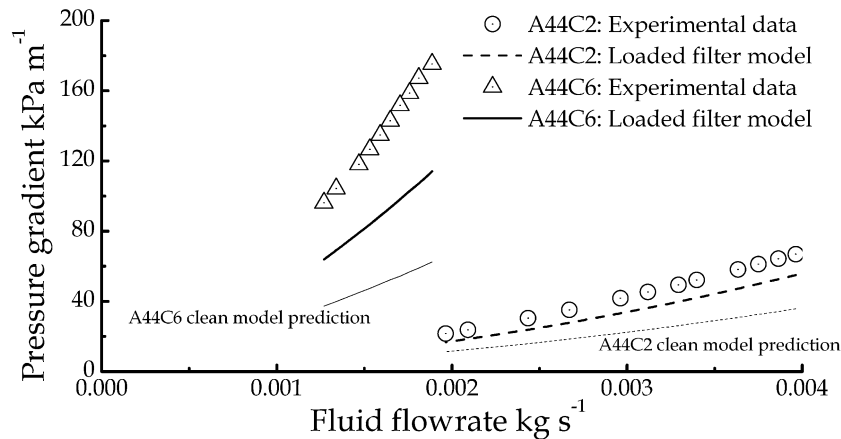

Fig. 15 Graph of pressure gradient versus fluid flowrate for PM-loaded ceramic foam filters, comparing model with experimental data

dependence of the pressure drop on the cell diameter, porosity, and filter surface area for given flowrates. This section shows how the models can be used to calculate optimum filter lengths and surface areas that correspond to target filtration efficiencies. From these results, a suitable geometry of gelcast foam filter for a passenger car diesel engine is calculated as an example of the models' use.

The engine used as an example for the analysis is a 2.0 l, four-stroke, four-cylinder, turbocharged, charge-cooled, direct injection, common rail diesel engine. A summary of the engine specification is shown in Table 3. The maximum engine exhaust

system back-pressure recommended by engine manufacturers for passenger cars is 20 kPa (gauge) [**34**, **35**]. For an exhaust temperature of 784 K and total back-pressure of 115 kPa (i.e. 75 per cent of the maximum back-pressure), the density ρ and viscosity μ of the gas are 0.51 kg/m^3 and 36.7×10^{-6} kg/m per s respectively.

6.1 Determination of filter length

The methodology for the determination of the optimum dimensions of the filter is first to determine the minimum filtration length that will meet the

Table 3 Engine specification and exhaust gas data

Engine type	Direct injection, common rail, turbocharged, charge-cooled, passenger car diesel engine
Displacement volume, cycle	2.0 l, four-stroke cycle
Exhaust gas flowrate at maximum power	0.14 kg/s
Exhaust temperature	784 K
Maximum exhaust back-pressure	20 kPa

recommended filtration efficiency of the gelcast ceramic foam. However, there is a lack of literature on filtration efficiency modelling with respect to ceramic foam filters and gelcast ceramic foams in particular. Consequently, reports that can reliably be considered and could be applicable to ceramic foam filter design are based directly on experimental results.

It can be recalled that in deep bed filtration the efficiency increases with the filter thickness (length), owing to the deep bed filtration in which the whole body of the filter acts to trap PM. Tutko *et al.* [**36**], Mizrah *et al.* [**37**], and most recently Hughes *et al.* [**22**] reported that filtration efficiency increases with filter thickness up to a point beyond which only modest gains in efficiency are noted. Hughes *et al.* [**22**] reported that the gelcast foam filter of length 30 mm yields filtration efficiency of > 75 per cent. They also reported that for a given superficial velocity, the filtration efficiency can be increased by > 30 per cent by decreasing the porosity from 94 to 87 per cent. Furthermore, they also demonstrated that the filtration efficiency can be increased by > 20 per cent by reducing the cell diameter by 100 μm. Considering the data from Hughes *et al.* [**22**], it was estimated that a gelcast foam filter of length 25 mm, cell diameter of 250 μm, and porosity of 85 per cent would have a filtration efficiency of ~ 85 per cent. This approximate filtration efficiency is reasonable for a DPF and, as such, an example application of the MOM model is presented to determine the optimum filter frontal area for this filtration thickness, pore diameter, and porosity. Complete optimization of filter design, including filtration thickness, would require more thorough knowledge and predictive capability of the filtration efficiency characteristics of the gelcast ceramic foams.

6.2 Correlating the pressure drop to the filter frontal surface area

Using the PM-loaded MOM model, the pressure drop across the foam filter was calculated for frontal surface areas ranging from 0.02 to 0.2 m² for PM loads of 0.2, 0.8, 1.3, 3.0, and 5.0 g/l. Using the calculated values, the pressure drop was plotted against the filter frontal surface area as shown in Fig. 16. Since the PM-loaded model was calibrated against 25 mm-thick test samples, the assumption of pressure drop being a function of average PM loading (as opposed to local PM loading and PM distribution) is considered to be suitable for this case. Considering conceptual filters of significantly
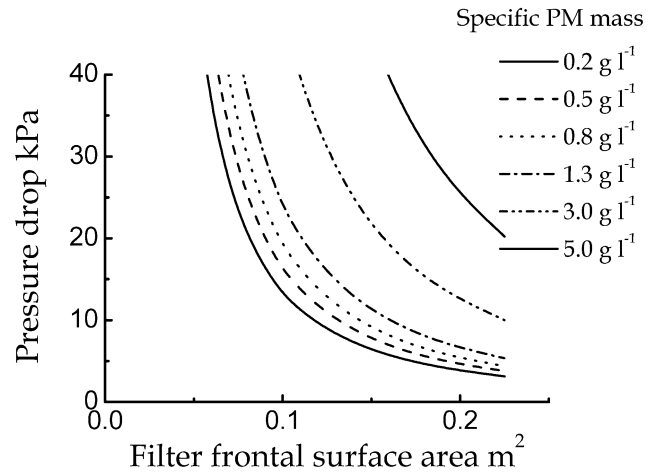
Fig. 16 Graph of pressure drop versus filter frontal surface area for various values of PM load, where the porosity and cell diameter of the foam are 85 per cent and 0.25 mm respectively

different filtration thickness (and hence filtration efficiency) the model would need to be applied in finite thickness sections to account for the distribution of PM through the filtration thickness.

The maximum engine back-pressure (i.e. 20 kPa) was projected on to the curves to give the values of minimum filter frontal surface area. For example, a PM load of 5.0 g/l corresponds to a frontal surface area of 0.225 m² and the PM load of 0.2 g/l corresponds to a surface area of 0.08 m².

Using the same procedure, the optimum surface filter frontal area with the above foam parameters for an exhaust flowrate of 0.14 kg/s and PM load of 2.5 g/l is 0.128 m². It should be noted that the PM loading is lower than for comparable WFFs. This is a characteristic of relatively small-pore diameter ceramic foam DPFs, for which the back-pressure is more sensitive to PM loading.

6.3 Gelcast ceramic foam filter configuration

Using the foam filter specification recommended for a PM load capacity of 2.5 g/l, a disc shape can be adopted where the filter diameter *D* is 404 mm, giving a frontal surface area of 0.128 m² and a total volume of 3.2 l. This is a larger package volume than a typical wall flow filter of length 144 mm and diameter 152 mm, which is 2.6 l.

However, a more compact shape of foam filter is the 'top hat' geometry suggested by Mizrah *et al.* [**37**]. Figure 17 shows the cross-section of a top hat design where the thickness of the foam is *L*. The total frontal surface area of the top hat can be defined with the expression
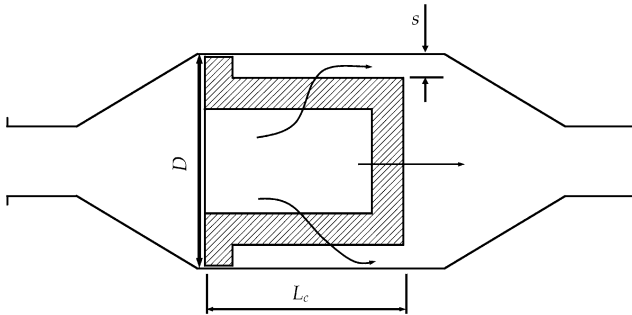
Fig. 17 Example of 'top hat' cross-section of ceramic foam DPF prototype

$$A_{\text{filt}} \geqslant \frac{\phi^2}{4}\pi + (L_{\text{c}} - L)(\phi - 2s - 2L)\pi \tag{57}$$

After fixing the filter diameter ϕ and the gap s, the inner canister length L_{c} can be selected to be able to contain the top-hat-shaped foam filter. For example, if the filter diameter is 200 mm and the gap s is 10 mm, then the length L_{c} is found to be 261 mm to achieve the frontal surface area of $0.128\,\text{m}^2$.

Other foam filter configurations were suggested by Gabathuler *et al.* [**38**]. They studied the performance of a variety of reticulated ceramic foam filter configurations, employing stationary engine as well as vehicle testing methods. One configuration was the Z-flow shape, which is not unlike large WFF geometry [**4**], although potential issues with even PM distribution within complex geometry foams need consideration. It can be seen that the gelcast ceramic foam can be shaped into almost any configuration to help meet the available space in the vehicle. If there is need to reduce further the filter volume, the PM load limit can be reduced or the filter thickness reduced. Another approach is to increase the cell diameter, which will reduce the pressure drop.

7 CONCLUSIONS

The new MOM model was developed from the fluid flow theory using conceptual multiple orifices to represent the complex structure of the gelcast ceramic foam filter. The relationship for viscous pressure losses is based on the Ergun relationship modified to suit gelcast ceramic foams and the kinetic pressure losses were accounted for by evaluating kinetic losses across numerous orifice restrictions.

A single constant in the model was calibrated using experimental data from rapid manufactured physical scale models of the cellular foam structures.

The calibrated model was then validated with experimental data from a number of foam samples. Predicted pressure gradients of the real ceramic foams were typically within 25 per cent of experimental values, importantly, without the need for recalibration on real foams.

Furthermore, a new mathematical model has been developed to predict pressure gradients of PM-loaded ceramic foam filters. This model was developed by adapting the MOM model to include the PM-loaded foam structure. The model was calibrated using experimental data from PM-loaded gelcast ceramic foam filter samples.

Finally, the MOM PM-loaded foam model was used to determine the optimum dimensions of a gelcast DPF for a passenger car 2.0 l, common rail diesel engine.

These models allow the prediction of back pressure in the exhaust system of a diesel engine fitted with a gelcast ceramic foam filter without the cost and time associated with producing and testing real samples.

REFERENCES

1 **Moran, J. P., Rumigny, J. F., Bion, A.,** and **Dionnet, F.** Isoflavones protect against diesel engine exhaust injury in organotypic culture of lung tissue. *Environ. Toxic. Pharmac.*, 2002, **12**, 213–220.

2 United States Environmental Pollution Agency. Air and radiation technical highlights, 2003 EPA420-F-03-017.

3 Swiss Agency for the Environment, Forest and Landscape (SAEFL). Particulate trap for heavy duty vehicles, 2000 Environmental Documentation No.

130. Available from http://www.umwelt-schweiz. ch/imperia/md/content/luft/fachgebiet/e/industrie/ Partikelfilter_UM130_e.pdf for further details (last accessed 17 November 2004).

4 **Howitt, J. S.** and **Montierth, M. R.** Cellular ceramic diesel particulate filter. SAE paper 810114, 1981.

5 **Kitagawa, J., Asami, S., Uehara, K.,** and **Hijikata, T.** Improvement of pore size distribution of wall flow type diesel particulate filter. SAE paper 920144, 1992.

6 **Itoh, A., Shimato, K., Komori, T., Okazoe, H., Yamada, T., Miimura, K.,** and **Watanabe, Y.** Study of SiC application to diesel particulate filter (part 1): material development. SAE paper 930360, 1993.

7 **Li, C. G., Mao, F., Swartzmiller, S. B., Wallin, S. A.,** and **Ziebarth, R. R.** Properties and performance of diesel particulate filters of an advanced ceramic material. SAE paper 2004-01-0955, 2004.

8 **Pyzik, A. J.** and **Li, C. G.** New design of a ceramic filter for diesel emission control applications. *Int. J. Appl. Ceram. Technol.*, 2005, **2**(6), 440–451.

9 **Konstandopoulos, A. G.** and **Johnson, J. H.** Wall-flow diesel particulate filters – their pressure drop and collection efficiency. *SAE Trans.*, 1989, **98**, paper 890405.

10 **Masoudi, M., Heibel, A.,** and **Then, P. M.** Predicting pressure drop of diesel particulate filters – theory and experiment. SAE paper 2000-01-0184, 2000.

11 **Konstandopoulos, A. G., Kostoglou, M., Skaperdas, E., Papaioannou, E., Zarvalis, D.,** and **Kladopoulou, E.** Fundamental studies of diesel particulate filters: transient loading, regeneration and aging. SAE paper 2000-01-1016, 2000.

12 **Hou, J. Z.** and **Angelo, T.** A new CFD model for understanding and managing diesel particulate filter regeneration. In Proceedings of the 10th Diesel Engine Emissions Reduction Conference 2004, Coronado, California (US Department of Energy).

13 **Bisset, E. J.** and **Shadman, F.** Thermal regeneration of diesel particulate monolithic filters. *AIChE J.*, 1985, **31**(5), 753–758.

14 **Law, M. C., Clarke, A.,** and **Garner, C. P.** A diesel particulate filter regeneration model with a multi-step chemical reaction scheme. *Proc. IMechE, Part D: J. Automobile Engineering*, 2005, **219**(D2), 215–226.

15 **Konstandopolous, A. G., Kostoglou, M., Housiada, P., Vlachos, N.,** and **Zarvalis, D.** Multichannel simulation of soot oxidation in diesel particulate filters. SAE paper 2003-01-0839, 2003.

16 **Ergun, S.** and **Orning, A. A.** Fluid flow through randomly packed columns and fluidised beds. *Ind. Engng Chemistry*, 1949, **41**, 1179–1184.

17 **Ergun, S.** Fluid flow through packed columns. *Chem. Engng Prog.*, 1952, **58**(2), 89–94.

18 **Innocentini, M. D. M., Salvini, V. R., Macedo, A.,** and **Pandolfelli, V. C.** Prediction of ceramic foams permeability using Ergun's equation. *Mater. Res.*, 1999, **2**(4), 283–289.

19 **Richardson, J. T., Peng, Y.,** and **Remue, D.** Properties of ceramic foam catalyst support: pressure drop. *Appl. Catalysis A: General*, 2000, **204**, 19–32.

20 **Pontikakis, G. N., Koltsakis, G. C.,** and **Stamatelos, A. M.** Dynamic filtration modeling in foam filters for diesel exhaust. *Chem. Engng Communs*, 2001, **188**, 21–46.

21 **Schmahl, J. R.** and **Davidson, N. J.** Ceramic foam filter technology for aluminium foundries. *Modern Casting*, 1993, **83**(7), 31–33.

22 **Hughes, S., Binner, J.,** and **Sambrook, R.** Dirty to desirable – gelcast ceramic foam diesel particulate filters (DPFs). In Proceedings of the American Ceramic Society (AcerS), 104th Annual Meeting, St Louis, Missouri, 26 April–1 May 2002.

23 **Davies, C. N.** *Air filtration*, 1973 (Academic Press, London).

24 **Brown, R. C.** *Air filtration: an integration approach to the theory and applications of fibrous filters*, 1993 (Pergamon Press, Oxford/New York).

25 **Tien, C.** and **Payatakes, A. C.** Advances in deep bed filtration. *AIChE J.*, 1979, **25**(5), 737–759.

26 **Sorenson, S., Hoj, J.,** and **Stobbe, P.** Flow characteristics of SiC diesel particulate filter materials. SAE paper 940236, 1994.

27 **Thomas, D., Contal, P., Renaudin, V., Penicot, P., Leclerc, D.,** and **Vendel, J.** Modelling pressure drop in HEPA filters during dynamic filtration. *J. Aerosol Sci.*, 1999, **30**(2), 235–246.

28 **Versaevel, P., Colas, H., Rigaudeau, C., Noirot, R., Koltsakis, G. C.,** and **Stamatelos, A. M.** Some empirical observations on diesel particulate filter modelling and comparison between simulations and experiments. SAE paper 2000-01-477, 2000.

29 **Tien, C.** and **Payatakes, A. C.** Advances in deep bed filtration. *AIChE J.*, 1979, **25**(5), 737–759.

30 **Peng, H. X., Fan, Z., Evans, J. R. G.,** and **Bustfield, J. J. C.** Microstructure of ceramic foams. *J. Eur. Ceram. Soc.*, 2000, **20**(7), 807–813.

31 **Macdonald, I. F., El-Sayed, M. S., Mow, K.,** and **Dullien, F. A. L.** Flow through porous media – the Ergun equation revisited. *Ind. Engng Chemistry Fundamentals*, 1979, **18**, 198–208.

32 **Sepulveda, P.** and **Binner, J. G. P.** Processing of cellular ceramics by foaming and *in situ* polymerisation of organic monomers. *J. Eur. Ceram. Soc.*, 1999, **19**, 2059–2066.

33 BS EN ISO 5167: Part 2: 2003. *Measurement of fluid flow by means of pressure differential devices inserted in circular cross-section conduits running full.*

34 **Mayer, A.** Definition, measurement and filtration of ultra fine solid particle emitted by diesel engines. In Proceedings of TTM, ATW–EMPA Symposium, 2002.

35 **Schnakenberg Jr, G. H.** and **Bugarski, A. D.** Review of technology available to the underground mining industry for control of diesel emission. US Department of Health and Human Services, DHHS (NIOSH), 2002, Publication No. 2002-154.

36 Tutko, J. J., Lesta, S. S., Brockmeyer, J. W., and **Dore, J. E.** Feasibility of ceramic foam as a diesel particulate trap. SAE paper 840073, 1984, pp. 15–24.

37 Mizrah, T., Maurer, A., Gauckler, L., and **Gabathuler, J.-P.** Open pore ceramic foam as diesel particulate filter. SAE paper 890172, 1989, pp. 19–27.

38 Gabathuler, J. P., Mizrah, T., Eckert, L., Fischer, A., Kaser, P., and **Maurer, A.** New developments of ceramic foam as a diesel particulate filter. SAE paper 910325, 1991.

APPENDIX

Notation

A	flow area (m^2)
A_{filt}	filter cross-sectional area (m^2)
A_{flow}	cross-sectional area of the fluid in the filter (m^2)
A_o	equivalent tube cross-sectional area (m^2)
A_w	window cross-sectional area (m^2)
A_1	flow area of foam cell (m^2)
A_2	flow area of window (m^2)
c_1, c_2	constants
d	cell diameter (m)
d_o	equivalent tube diameter (row of cells, in m)
D	filter diameter (m)
g_1	constant for gradient of PM loading profile
h	truncation length of a pore by a neighbouring cell
k	ratio of window diameter to cell diameter, w/d
k_n	constant for edge profile of PM loading
L	length of filter (m)
L_c	inner canister length
m'	mass fluid flowrate (kg/s)
M	number of cell in a row of cells across filter
N	number of cell per unit volume of filter
N_{row}	number of rows of cells in a cross-sectional area of filter
$p_1, p_2, p_3 \ldots p_n$	gas pressures (Pa)
q	flowrate through row of cells (m^3/s)
Q	volumetric fluid flowrate (m^3/s)
r	cell radius
r_1	perpendicular distance from PM surface to centre of the cell
Re	Reynolds number
S	wetted surface area of a cell (m^2)
S_{TR}	surface area truncated by a neighbouring cell (m^2)
S_V	specific surface area (m^{-1})
u	superficial velocity (m/s)
$u_1, u_2, u_3, \ldots, u_n$	fluid velocities in cells (m/s)
V_{arc}	volume swept by an arc around the cell axis
V_C	volume truncated by neighbouring cells (m^3)
V_{CELL}	volume of cell (m^3)
V_{line}	volume swept by a line around the cell axis
V_{mat}	volume of filter material (m^3)
V_p	PM volume in filter (m^3)
V_{PM}	volume of PM deposit per filter cell (m^3)
V_S	volume of sphere cell (m^3)
w	window diameter (m)
w'	window radius
α	Ergun's correction factors applied on viscous loss
β	kinetic correction coefficient
Δp	pressure drop (Pa)
Δp_{kin}	pressure drop from kinetic energy loss (Pa)
Δp_{vis}	pressure drop from viscous energy loss (Pa)
ε	porosity
ε_n	loaded filter porosity
ε_p	deposited PM porosity
θ	angle of PM surface relative to flow cross-section
μ	viscosity of the fluid (kg/m per s)
ρ	fluid density (kg/m^3)
σ	PM specific volume in filter (m^3 PM per m^3 filter)
ψ	angle of inclination of PM deposit in filter (rad)

Abbreviations

CAD	computer-aided design
DPF	diesel particulate filter
EEM	extended Ergun mathematical (model)
EPA	environmental protection agency
MOM	multiple orifice mathematical (model)
PM	particulate matter
SEM	scanning electron microscopy (or microscope)